

Article

Copper, Uranium and REE Mineralisation in an Exhumed Oil Reservoir, Southwest Orkney, Scotland

Eleanor A. Heptinstall¹, John Parnell¹, Joseph G. T. Armstrong^{1,*}, Andrea Schito¹
and Temitope O. Akinsanpe^{1,2}

¹ School of Geosciences, King's College, University of Aberdeen, Aberdeen AB24 3UE, UK; e.heptinstall.18@abdn.ac.uk (E.A.H.); j.parnell@abdn.ac.uk (J.P.)

² Department of Geology, Obafemi Awolowo University, Ile-Ife 220103, Nigeria

* Correspondence: joseph.armstrong@abdn.ac.uk

Abstract: Copper, uranium, and rare earth element (REE) mineralisation occurs in hydrocarbon-bearing Devonian continental sandstones in southwest Orkney, Scotland. The aeolian Yesnaby Sandstone Formation and fluvial Harra Ebb Sandstone Formation were mineralised following oil emplacement. The REE-bearing APS mineral florencite is particularly associated with bituminous nodules, many of which contain brannerite. Subsequently hydrothermal copper and other sulphides, and barite, further mineralised the oil reservoir at a temperature of ~190 °C. Oil was mobilised through mineralised fractures at this stage. Biodegradation of the oil occurred later, following the Carboniferous-Permian uplift. The occurrence confirms that Cu-APS mineralisation is possible in relatively low-temperature regimes in sedimentary basins.

Keywords: Cu-U-REE mineralisation; APS minerals; Orcadian Basin; florencite; biodegradation; hydrocarbons; bitumen



Citation: Heptinstall, E.A.; Parnell, J.; Armstrong, J.G.T.; Schito, A.; Akinsanpe, T.O. Copper, Uranium and REE Mineralisation in an Exhumed Oil Reservoir, Southwest Orkney, Scotland. *Geosciences* **2023**, *13*, 151. <https://doi.org/10.3390/geosciences13050151>

Academic Editors: Paul Alexandre and Jesus Martinez-Frias

Received: 25 February 2023

Revised: 16 May 2023

Accepted: 16 May 2023

Published: 20 May 2023



Copyright: © 2023 by the authors. Licensee MDPI, Basel, Switzerland. This article is an open access article distributed under the terms and conditions of the Creative Commons Attribution (CC BY) license (<https://creativecommons.org/licenses/by/4.0/>).

1. Introduction

An exhumed oil reservoir occurs in Devonian fluvial-aeolian sandstones in southwest Orkney, Scotland [1–3]. The reservoir was previously known to host U-bearing minerals [4–6] and is shown here to additionally host copper-uranium-rare earth element (Cu-U-REE) mineralisation. Copper mineralisation occurs in exhumed oil reservoirs in several basins, e.g., [7–12]. However, the combination with REE-bearing APS (aluminium phosphate sulphate) minerals, mostly florencite in this case, is unusual in sedimentary rocks.

Aluminium phosphate sulphate (APS) minerals are common accessory products in a range of volcanic, hydrothermal, sedimentary, and metamorphic systems, occurring under a wide range of pH, redox and oxygen fugacity conditions [13]. APS minerals have been widely documented in Cu-mineralised systems [13], including porphyry-copper ores [14,15], epithermal deposits [15–17] and along uranium-mineralised unconformities [18,19]. REE-bearing APS minerals hosted in carbonaceous rocks are limited but have been documented in black shales [20]. Examples of a range of copper-mineralised systems which contain APS minerals are given in Table 1. They consistently formed at temperatures above 200 °C, and hence do not normally show any relationship with organic matter. In this account, we report an example of APS minerals with U and Cu mineralisation at lower (<200 °C) temperatures.

This study examines petrographic relationships at Yesnaby in the Devonian Orcadian Basin, Orkney. The relationships are assessed in terms of:

- (i) The spatial relationships between mineralisation and hydrocarbons,
- (ii) The paragenetic relationships between mineralisation and hydrocarbons,
- (iii) The timing of mineralisation and hydrocarbon emplacement within the burial/uplift history.

Table 1. Occurrences of APS minerals in copper deposits with their formation temperature constraints.

Locality	Age	Host Rock	Key Minerals	Temp. (°C)	References
Asarel, Bulgaria	Cretaceous	Porphyry	florencite, chalcopyrite	>394	[21]
Chelopech, Bulgaria	Cretaceous	Metavolcanics	florencite, tennantite-chalcopyrite	200–300	[22]
Shituru, D. R. Congo	Neoproterozoic	Metasediment	florencite, chalcopyrite	~430	[23]
Singhbhum copper belt, India	Proterozoic	Metasediment	florencite, chalcopyrite	~490	[24]
Olympic Dam-Oak Dam, Australia	Proterozoic	Brecciated granite and metasediments	florencite, chalcopyrite-bornite	150–400	[25,26]
Oyu Tolgoi, Mongolia	Devonian	Porphyry	florencite, bornite	>260	[27]
Summitville, Colorado, USA	Miocene	Epithermal/volcanics	Svanbergite, covellite-chalcopyrite	~250	[28]
La Granja, Peru	Miocene	Porphyry	woodhouseite, chalcopyrite	260–350	[28]
Safyanovskoe, Urals, Russia	Devonian-Carboniferous	Altered volcanics	goyazite, chalcopyrite	<250	[29]
Melitena, Greece	Eocene-Miocene	Epithermal/porphyry	woodhouseite-svanbergite, chalcopyrite	~300	[30]
Athabasca, Canada	Palaeoproterozoic	Unconformity uranium deposit	florencite, chalcopyrite	230–240	[17]

2. Geological Setting

In this case study we investigate the continental Devonian (Lower Old Red Sandstone) sedimentary rocks at Yesnaby in south-west Orkney (Figure 1). These sandstones unconformably overlie a crystalline basement which is comprised of Caledonian granite, biotite schist, hornblende schist and gneiss [4,31]. Caledonian granite intrusions are dated using U-Pb analysis to the Scandian Orogeny, approx. 432–430 Ma [32].

At Yesnaby, an exhumed oil reservoir of Devonian aeolian sandstones is well exposed [1–3], unconformably overlying the basement. Two stratigraphic units, the fluvial-breccia Harra Ebb Sandstone Formation and the overlying aeolian Yesnaby Sandstone Formation (Figure 1), pass upwards into a cyclic sequence of organic-rich lacustrine shales and sandstones attributed to the Yesnaby Flagstone Group [1]. The Devonian succession in Orkney was previously documented to have experienced a maximum burial temperature of about 150 °C [3,33,34], and hydrocarbons were generated from the lacustrine shales [35]. However, greater temperatures attributed to hydrothermal fluids are under-explored.

The Devonian rocks in the vicinity of the unconformity are mineralised by lead-zinc and uranium, and thermal reactivation of the granitic pluton beneath is strongly implicated as the source of heat and metals for mineralisation [36,37], though there is no clear evidence of an associated magmatic event. The mineralisation consists of lead-zinc sulphides (galena, sphalerite) in the lacustrine shales [38–40], and uranium oxides (uraninite, brannerite) in sandstones and fault breccias [1,6]. The lead-zinc mineralisation has been interpreted as early diagenetic, due to its association with algal structures and cherts [38–40]. In contrast, the uranium mineralisation occurred later, as evidenced by its association with fault zones and hydrocarbons [1,5,6,36].

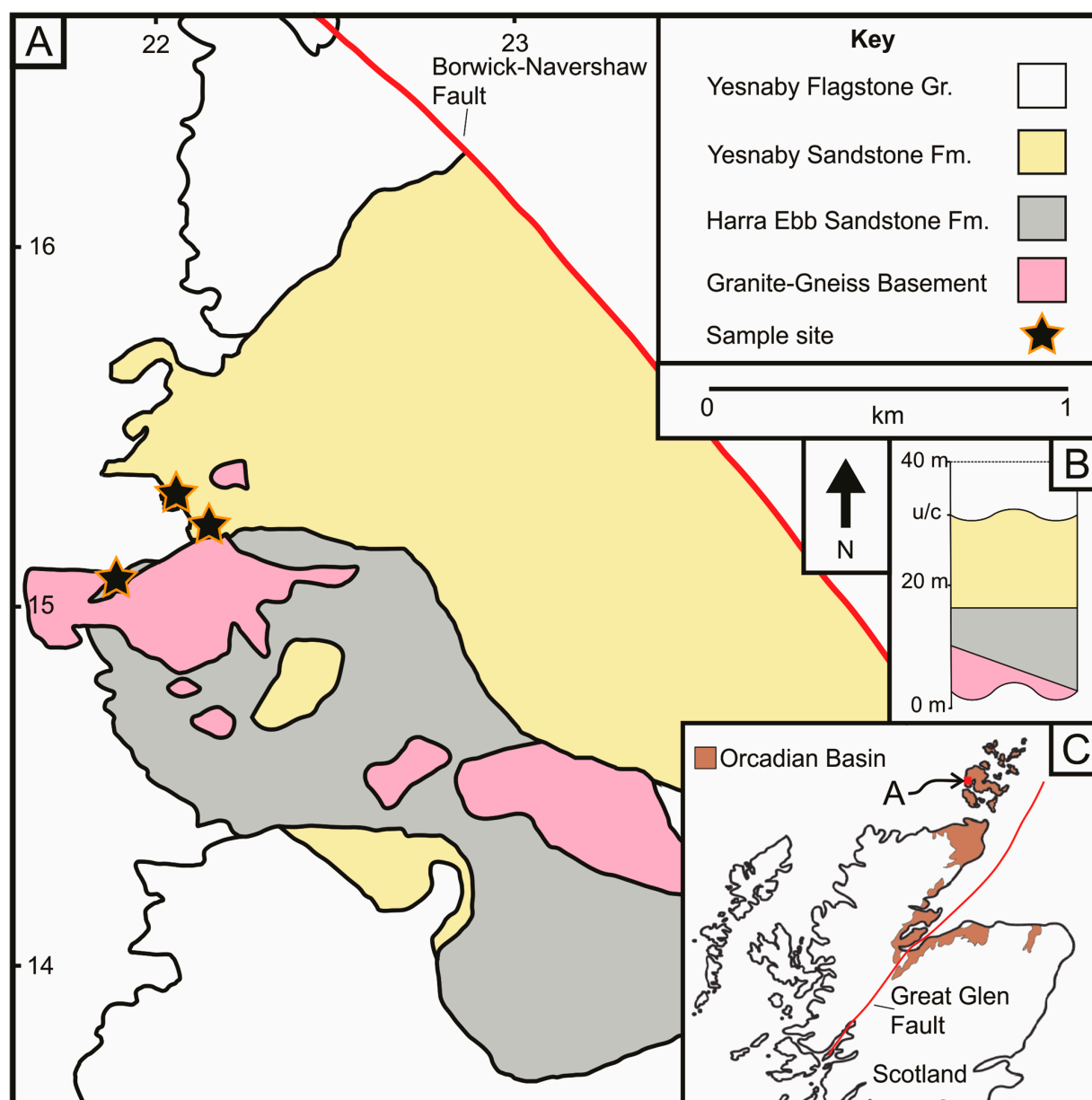


Figure 1. (A) Simplified geological map of the Harra Ebb and Yesnaby sandstone formations, which overlie granite-gneiss basement rocks, which is intercepted by the Borwick-Navershaw Fault (after [3]). The sampling sites are shown by the stars. British National Grid reference lines for grid square HY shown. (B) Inset simplified stratigraphic figure illustrates the Granite-Gneiss basement, overlying Lower Devonian Harra Ebb and Yesnaby fluvial-aeolian sandstones, that are below the Lower Devonian unconformity (u/c) and overlying Yesnaby Flagstone Group rocks (after [3]). (C) Inset map showing the Yesnaby location in the Orkney Islands, that form part of the wider Devonian Orcadian Basin outcrops, shown in brown (after [1]).

3. Materials and Methods

High-resolution image analysis was performed at the University of Aberdeen ACEMAC Facility using a Zeiss Gemini field emission gun scanning electron microscope (FEG-SEM) on polished blocks of the bitumen nodule-bearing sandstone. Samples were carbon coated and analysed at 20 Kv, with a working distance of 10.5 mm. Samples were analysed using Oxford Instruments EDS X-ray analysis. The standards used were a mixture of natural minerals, metal oxides and pure metals, as calibrated by the factory. Oxygen contents were determined by stoichiometry.

Fluid inclusion studies were performed on doubly polished wafers using a Linkam THMS-600 heating–freezing stage mounted on a Nikon Labophot transmission light microscope. The instrument equipped with a range of objective lenses including a 100× lens, was calibrated against synthetic H₂O (374.1 and 0.0 °C) and CO₂ (−56.6 °C) standards (Synthetic Fluid Inclusion Reference Set, Bubbles Inc., Los Angeles, CA, USA).

Biomarker extractions from bitumen residue were achieved with DCM/methanol (MeOH) (9/1, *v/v*) using a DIONEX Accelerated Solvent Extractor (ASE-200). The resulting solvents were then transferred into clean vials with a pipette. These steps were repeated with a solvent mix of DCM and MeOH (3/1, *v/v*) and 100% DCM. The solvent filtrates were accumulated into the second vial and left to dry in the fume cupboard at room temperature. The filtrates from ASE were dried down by Grant rotary evaporator and further transferred into vials. The dried extracted organic matter (EOM) from ASE and ME was separated into aliphatic, aromatic, and polar fractions by silica column chromatography using hexane, hexane/DCM (3/1, *v/v*), and DCM/MeOH (2/1, *v/v*), respectively. An internal standard (5β-Cholane, Agilent Technologies, Santa Clara, CA, USA) was added before injecting it into the gas chromatography-mass spectrometry instrument. Analysis used an Agilent 6890N gas chromatograph fitted with a JandW DB-5 phase 50 m MSD and a quadrupole mass spectrometer operating in scan and selected ion monitoring (SIM) mode (dwell time 0.1 sec per ion and ionisation energy 70 eV). The samples were injected manually using a split/splitless injector operating in splitless mode (purge 40 mL min^{−1} for 2 min). The temperature programme for the GC oven was 80–295 °C, holding at 80 °C for 2 min, rising to 10 °C min^{−1} for 8 min and then 3 °C min^{−1}, and finally holding the maximum temperature for 10 min^{−1}. Quantitative biomarker data were obtained for n-alkanes and acyclic isoprenoids, measured on the charge-to-mass ratio (*m/z*) 85; hopanes (*m/z* 191) and steranes (*m/z* 217 and 218). Thermal maturity was estimated from the 20S/(20S + 20R) ratio for the C29 steranes, and 22S/(22S + 22R) ratio for the C31 hopanes [41].

A Renishaw inVia reflex Raman spectrometer was used for the micro-Raman analysis of unpolished bitumen nodules, with a backscattering geometry in the range of 700–3200 cm^{−1} (first- and second-order Raman spectra), with a 2400 l mm^{−1} spectrometer grating and CCD detector under a maximum of ×50 confocal optical power (numerical aperture (NA) of the lens of 0.90). The slit opening was 65 μm with a CCD area of c. 10 pixels (80% of the total signal height hitting the CCD chip) and a confocal hole of 200 μm. A 514.5 nm diode laser was used for excitation with an output of 50 mW. Optical filters (1%) were used to adjust the power of the laser to less than 0.5 mW. Raman backscattering was recorded after an integration time of 20 s for three repetitions for each measurement. The Raman system was calibrated against the 520.7 cm^{−1} band of silica. The maximum temperature was derived using the automatic method of [42], designed to compare Raman data at different stages of thermal maturity from about 150 to 700 °C. It is based on the IFORS software that curve-fits Raman spectra of carbonaceous material, modelling simultaneously the background with a fifth-order polynomial curve and the Raman signal with pseudo-Voight bands [42,43]. The normalised intensities of the D and G bands (STA-D, STA-G) were used to calculate palaeotemperature by means of the third-degree polynomial equation proposed in [43].

A representative sample of Cu-mineralised Yesnaby sandstone was analysed for bulk elemental abundances using method ME-MS61L at ALS Laboratories, Loughrea, Ireland. Samples were initially crushed and homogenised using a tungsten TEMA mill followed by four-acid digestion using a graphite heating block. Samples were subsequently neutralised and analysed using inductively coupled plasma mass spectrometry (ICP-MS) and inductively coupled plasma atomic emission spectrometry (ICP-AES).

The sulphur isotope composition of pyrite in the Yesnaby sandstone was determined at the Scottish Universities Environmental Research Centre (SUERC), East Kilbride. Samples of pyrite were extracted from the sandstone using a diamond drill bit. Powdered sulphides were heated to combustion in the presence of excess copper oxide inside a high-vacuum line to produce sulphur dioxide (SO₂). Following separation from all other gaseous phases, the

resultant SO₂ was analysed for the ³⁴S and ³²S isotope concentrations using a VG Isotech SIRA II mass spectrometer, with a reproducibility of <0.2‰. Data are denoted as per mille (‰) difference relative to the industry standard Vienna-Canyon Diablo Troilite (V-CDT).

4. Results

4.1. Sandstone Petrology

The Yesnaby Sandstone Fm and Harra Ebb Sandstone Fm primarily comprise a detrital mineralogy of K-feldspar, quartz and in Yesnaby sandstones, minor muscovite. The accessory heavy minerals identified in the Yesnaby and Harra Ebb sandstones are monazite and zircon, but their occurrence is rare due to the aeolian depositional environment. Both the Yesnaby and Harra Ebb sandstones host minerals and clays consistent with diagenetic mineral alteration, including quartz overgrowths, illite and calcite. These secondary illite and quartz overgrowths are observed infilling porosity between detrital K-feldspar grains (Figure 2). Evidence of hydrocarbon migration is widespread in both the Yesnaby and Harra Ebb sandstones, with abundant bitumen-filled and partially-filled pore spaces. Later mineralisation occurs at the rims of pore-filling bitumen and vacant pores.

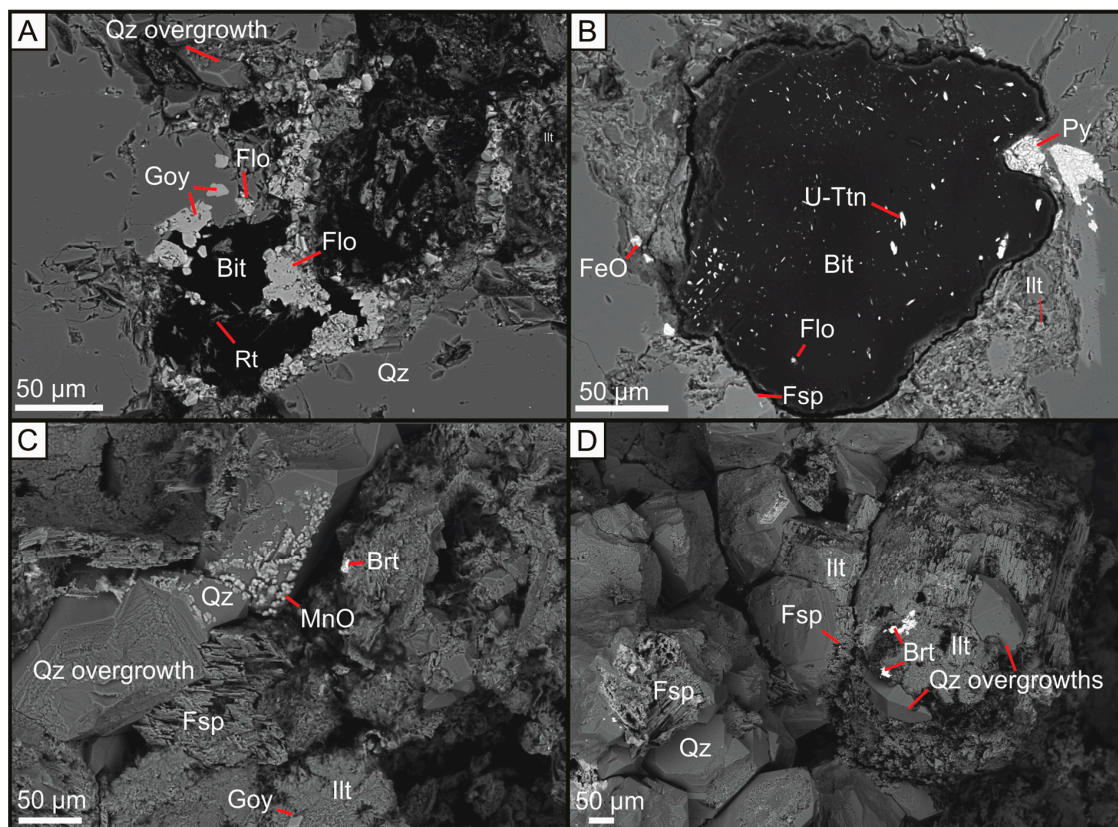


Figure 2. Backscattered electron micrographs of APS mineralisation in or around the rims of bituminous nodule, and quartz overgrowths associated with feldspar overgrowths, illite, and manganese and barite mineralisation. (A) U-poor bitumen nodule from the Harra Ebb Sandstone Fm nodule associated with LREE-rich florencite and Sr-rich goyazite; (B) Brannerite-bearing bitumen from the Harra Ebb Sandstone Formation associated with pyrite, feldspar, illite and nodule-hosted florencite; (C) Yesnaby Sandstone Fm quartz overgrowths associated with Mn-oxide mineralisation, feldspar, barite mineralisation and illite with Sr-rich goyazite; (D) Yesnaby Sandstone Fm quartz overgrowths associated with illite, barite mineralisation, that fill the remaining porosity between detrital quartz and feldspar. Bit = Bitumen, Rt = Rutile, U-Ttn = Uranium-titanate (Brannerite), Flo = Florencite, Py = Pyrite, FeO = Iron oxide/hydroxide, Qz = Quartz, Illt = Illite, Goy = Goyazite, Brt = Barite, Fsp = Potassium Feldspar, MnO = Manganese oxide.

Uraniferous-titanium and titanium oxide minerals are widespread in the Harra Ebb Sandstone within bitumen nodules and less frequently in Yesnaby sandstones. Late-stage illite mineralisation is associated with Aluminium Phosphate Sulphate (APS) minerals in these formations. Where the associated illite is pore-filling, the APS mineral compositions are wide-ranging, but the mineralogy is most commonly Sr-S-APS. Where the associated illite is forming rims around bitumen nodules, the APS minerals are LREE-rich. Pyrite and calcite also occur in association with hydrocarbon rim-fill illite with APS minerals. Supergene alteration of pyrite to Fe-oxide or Fe-hydroxide is common at these sites. Sr-S-APS minerals in the Yesnaby Sandstone Fm are commonly dolomite cemented.

Cross-cutting veins of barite and sulphides (Figure 3), containing fragments of remobilised bitumen, are common in the Yesnaby Sandstone Fm, while these are rare in the Harra Ebb Sandstone. These vein assemblages are often dolomite cemented, with supergene alteration of copper-sulphides to malachite.

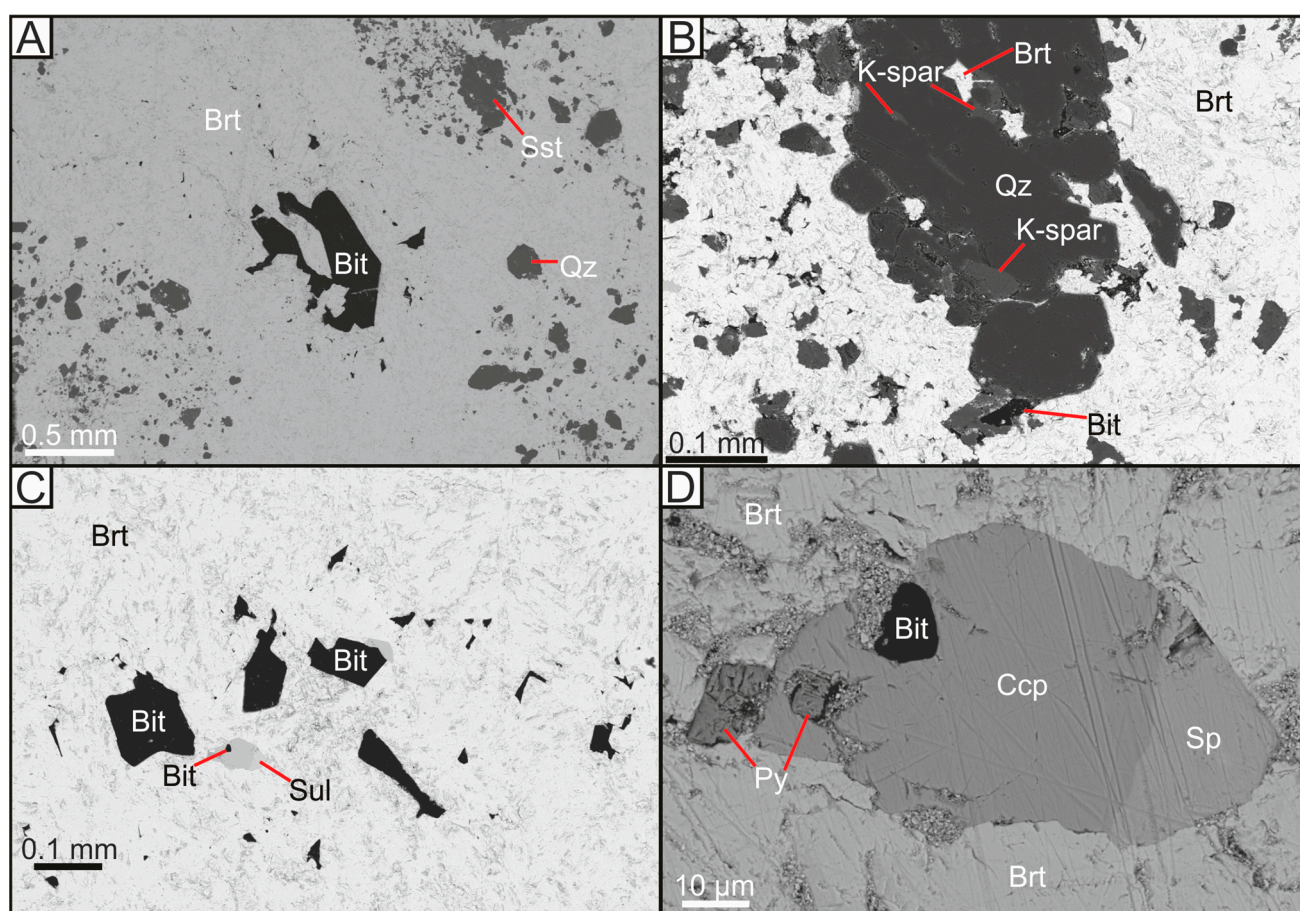


Figure 3. Backscattered electron micrographs of copper-barite-bitumen veining within Yesnaby sandstone. (A) Barite vein with inclusions of bitumen and sandstone; (B) Barite vein with inclusions of brecciated sandstone minerals; (C) Bitumen and various sulphide inclusions within barite; (D) Sulphide overgrowths around bitumen inclusion, within barite vein. Bit = Bitumen, Brt = Barite, Ccp = Chalcopyrite, K-spar = Potassium Feldspar, Py = Pyrite, Qz = Quartz, Sp = Sphalerite, Sst = Host Sandstone, Sul = Sulphides.

Whole rock analysis of the Yesnaby sandstone identified that the copper concentration in a representative sample exceeds 1 wt.%, which demonstrates the copper-rich nature of these lithologies due to their mineralisation. The sulphur-isotope ratio ($\delta^{34}\text{S}$) of the sulphides (pyrite) in the Yesnaby sandstone is +10.6‰.

4.2. Mineralisation

APS minerals in the Yesnaby Sandstone Formation and Harra Ebb Sandstone Formation occur as discrete grains ranging from sub-micron to 50 microns in size. Most APS grains have a rhombohedral crystal shape, although larger APS grains can have a sub-rounded shape (Figure 2A). The APS minerals are commonly found at the periphery of bitumen nodules within an illite matrix, and less commonly within the nodules (Figure 2B). Illite-hosted APS grains usually have a size range of 5–15 microns.

APS minerals have compositions that vary from Sr-rich to LREE-rich (Table 2), referable to goyazite or florencite-type, respectively. LREE-rich APS grains recorded here as florencite show a total (LREE)₂O₃ content of up to 9.94 wt.%, whilst Sr-rich APS grains recorded as goyazite, contain traces of LREE, typically <1 wt.% (LREE)₂O₃ (Table 2). Where APS minerals surround the rim of or are entrained within bitumen nodules, they are more likely to have a composition comparable to florencite. Deviations from the ideal formulae for florencite and goyazite suggest that the minerals belong to a solid solution series between these end members.

Table 2. Sr-LREE-S and major element oxide compositions of analysed APS minerals. (1–7) LREE-rich florencite composition. (8–10) Sr-rich goyazite composition. bdl = Below Detection Limit.

Oxide (wt.%)	Florencite							Goyazite		
	1	2	3	4	5	6	7	8	9	10
Na ₂ O	bdl	0.38	bdl	bdl	bdl	bdl	bdl	bdl	bdl	bdl
FO	bdl	0.38	bdl	bdl	bdl	bdl	bdl	2.57	bdl	1.93
Al ₂ O ₃	30.83	29.9	34.92	33.74	30.83	34.92	31.89	35.42	31.88	34.54
SiO ₂	9.53	20.59	bdl	bdl	9.53	bdl	8.21	bdl	3.55	bdl
P ₂ O ₅	19.12	19.61	23.72	25.02	19.12	23.72	20.16	30.27	25.19	25.03
SO ₃	4	4.53	4.83	4.05	4	4.83	4.11	2.62	5.6	5.93
K ₂ O	0.63	bdl	bdl	bdl	0.63	bdl	0.49	bdl	0.24	bdl
CaO	1.68	1.54	1.02	0.19	1.68	1.02	1.61	0.28	0.45	0.41
SrO	11.65	12.57	15.54	16.06	11.65	15.54	11.37	21.96	20.66	21.09
La ₂ O ₃	3.35	2.53	3.41	2.48	3.35	3.41	3.35	bdl	bdl	bdl
Ce ₂ O ₃	5.14	4.24	5.47	4.74	5.14	5.47	5.6	bdl	0.38	bdl
Pr ₂ O ₃	bdl	0.57	bdl	bdl	bdl	bdl	bdl	bdl	bdl	bdl
Nd ₂ O ₃	1.01	0.73	1.06	1.09	1.01	1.06	0.9	bdl	bdl	bdl
ThO ₂	bdl	bdl	0.67	bdl	bdl	0.67	0.63	bdl	bdl	Bdl
Total (LREE) ₂ O ₃	9.5	8.07	9.94	8.31	9.5	9.94	9.85	bdl	0.38	bdl
Sum	86.94	97.57	90.64	87.37	86.94	90.64	88.32	93.12	87.95	88.93

Uranium-bearing, titanium minerals occur within rounded bitumen nodules up to 1 mm in diameter, although the majority are several tens of microns in diameter (Figure 2B). These minerals are described as a form of uranium-titanate (U-Ttn), which tend to be elongate, either distributed randomly or in clusters throughout the bitumen (Figure 2A). These U-Ttn minerals exhibit variable amounts of uranium (up to 40 wt.%), titanium (up to 22 wt.%), and minor Pb (up to 1.5 wt.%), Th (~1 wt.%) and Zr (up to ~4 wt.%). These mineral compositions are comparable to uraniferous leucoxene (UTiO₂) or brannerite (UTi₂O₆), as documented by [6] and will be referred to as brannerite for the purposes of this discussion. Brannerite minerals are accompanied by non-uraniferous titanium oxide, most likely rutile, that is up to 1 mm in diameter (Figure 2A). Distinct trace element oxide enrichments occur in each of the titanium minerals, including vanadium (present as V₂O₅) in brannerite and niobium (present as Nb₂O₃) in rutile (Supplementary Information 1). The brannerite mineralisation is described in detail by [6]. Bitumen typically has an S content of 1–3.5 wt.% and irregular U contents of <1 wt.%.

Uraniferous bitumen commonly shows contraction cracks (Figure 2B) around the nodule rim. U-poor bitumen usually has a smooth texture, commonly with rutile grains

(10–30 μm) nearer the nodule rim (Figure 2A). U-Ttn-bearing bitumen nodules are commonly accompanied by pyrite, illite and APS grains in the nodule rim (Figure 2B).

Authigenic quartz grains in the Yesnaby Sandstone Fm commonly have coatings of manganese oxide (Figure 2C). Large (~100 micron) diagenetic quartz overgrowths commonly surround K-feldspar, which was subsequently replaced by illite (Figure 2D). Barite and bitumen mineralisation (Figure 3A) include K-feldspar (Figure 3B), illite (Figure 2C,D) and quartz, and fill the remaining open pore space (Figure 3B). The cross-cutting vein assemblage through the sandstone (Figure 3) is dominated by barite, sulphides, (including pyrite, chalcopyrite (Figure 3C,D), and sphalerite (Figure 3D)), dolomite and remobilised bitumen fragments. The bitumen-barite veins likely post-date the formation of bitumen nodules (Figure 4A), nodule-associated APS (Figure 2A,B), pyrite and illite (Figures 2B and 4A). The barite also contains fragments of sandstone (Figure 3A), which are identical to the host sandstone, cemented with quartz overgrowths (Figure 3B) and infilled by bitumen (Figure 4B). Chalcopyrite is the predominant sulphide, that gives rise to a green colouration in the field due to the replacement of malachite during weathering stage (Figure 4B). SEM EDX analysis of the chalcopyrite and sphalerite shows that they have simple sulphide chemistries, with no trace elements or zonation. Pyrite within these barite veins contains minor concentrations of arsenic (0.5–5%), copper (trace) and cobalt (trace). Cross-cutting relationships suggest that the chalcopyrite, sphalerite and pyrite formed coeval with barite veining, partially replacing an earlier phase of pyrite mineralisation (Figure 3D). The sulphide minerals are 10–100 μm in size, with chalcopyrite commonly forming the largest sulphide minerals.

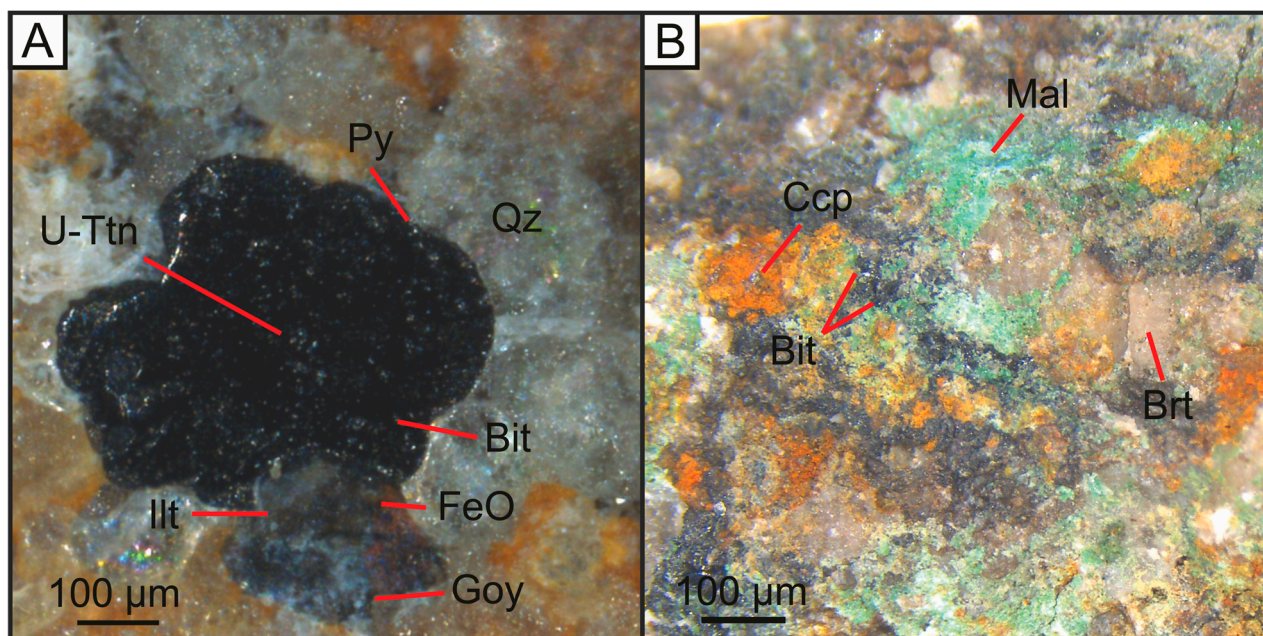


Figure 4. Optical microscopic images of (A) U-Ttn bearing bitumen nodule that fills sandstone porosity; (B) Cu-bearing, bitumen-barite vein that cuts sandstone country rock. Bit = Bitumen, U-Ttn = Uranium-titanate, Py = Pyrite, Qz = Quartz, FeO = Iron Oxide, Illite = Illite, Goy = Goyazite, Brt = Barite, Ccp = Chalcopyrite, Mal = Malachite.

4.3. Fluid Inclusions

The quartz overgrowths contain primary two-phase fluid inclusions (Table 3). The inclusions have both aqueous and hydrocarbon (oil) compositions. The hydrocarbon inclusions are distinguished by yellow fluorescence under ultra-violet light. The homogenisation temperatures for the two populations are in the range 119 to 138 $^{\circ}\text{C}$ and 122 to 136 $^{\circ}\text{C}$, respectively. The hydrocarbon inclusions are larger (up to 15 microns) than the aqueous inclusions (up to 8 microns). The aqueous inclusions have freezing (final melting) tempera-

tures in the range of -6 to -4 °C, corresponding to salinities of 7.6 to 9.3 wt.% equivalent to NaCl.

Table 3. Data for primary two-phase inclusions in quartz overgrowths, Yesnaby Sandstone, Orkney.

Population	1	2
Composition	Aqueous	Hydrocarbon
No. analysed	15	13
Size (μm)	4–8	5–15
Degree of fill	0.93 to 0.96	0.85 to 0.90
Homogenisation temp. (°C)	119.7 to 138.4	122.0 to 136.4
Freezing temp. (°C)	-6.1 to -4.1	-
Salinity (wt.% equiv. NaCl)	7.6 to 9.3	-
Fluorescence	None	Yellow

4.4. Raman Spectroscopy

Raman spectra of pore-filling bitumen nodules and bitumen in hydrocarbon veins are characterised by the presence of well-developed D and G bands in the first-order region, between 1200 and 1700 cm^{-1} and also by the presence of broad bands in the second-order region between 2700 and 3100 cm^{-1} (Figure 5). All spectra are characterised by a weak fluorescence that mainly affects the second-order region. The presence of some weak bands in the second-order region and of a small “shoulder” of the D band at around 1250 cm^{-1} are characteristic of spectra at the boundary between diagenesis and the low anchizone (sensu Frey and Robinson, 1998). Eighteen spots were measured to calculate average temperatures (Table 4) using the methodology of [42,43]. Raman-derived temperatures for both nodule and vein bitumen range between about 170 and 210 °C with an average value of 195.5 ± 18 °C (Table 4).

Table 4. Raman-derived temperatures using method in [42] for bitumen (nodules and veins).

Measurement	Temperature (°C)	Average T (°C)	std T (°C)
1	174		
2	199		
3	216		
4	164		
5	223		
6	209		
7	187		
8	167		
9	211		
10	205	195.5	18.52582
11	203		
12	194		
13	204		
14	168		
15	194		
16	177		
17	215		
18	209		

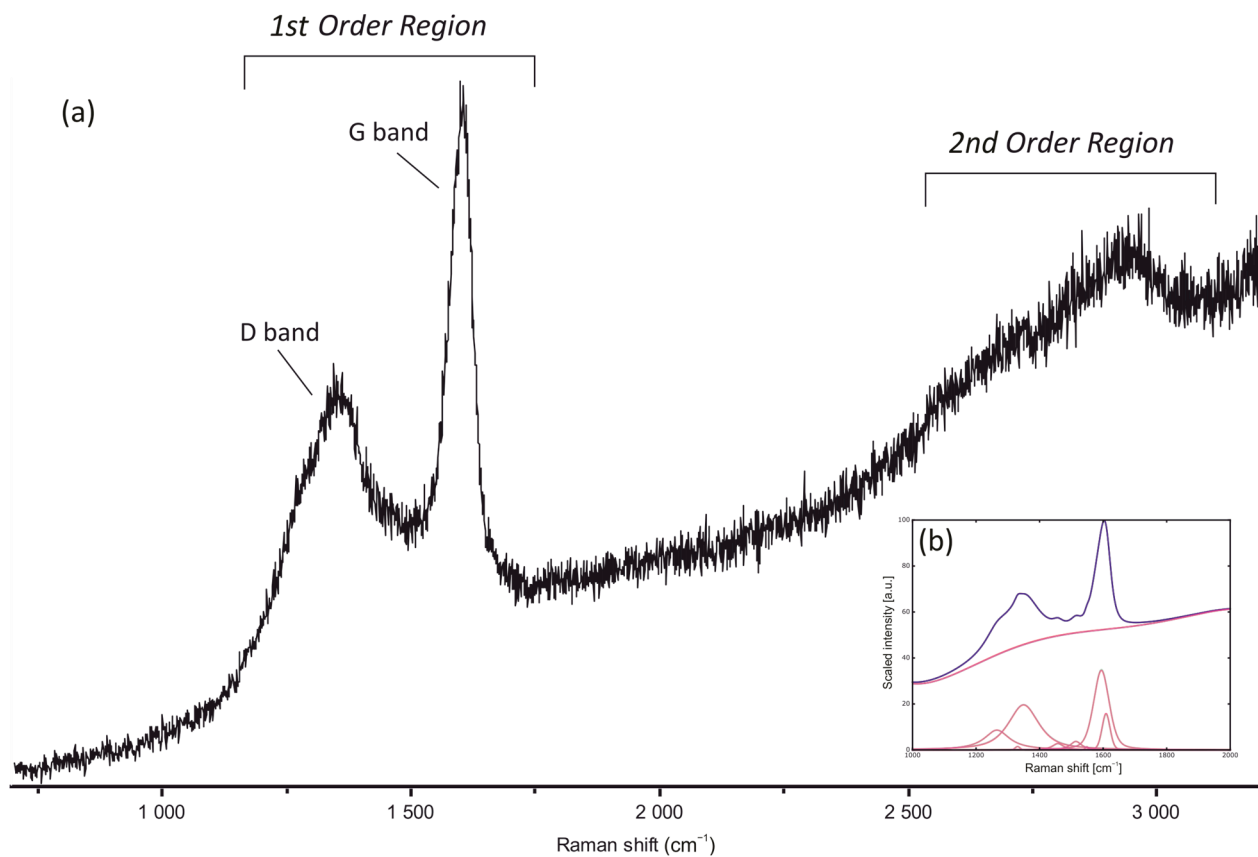


Figure 5. (a) Example of bitumen Raman spectra from hydrocarbon veins showing the presence of the D and G bands in the first order region and broad bands in the second order region; (b) example of the deconvolution using the IFORs software [42].

4.5. Gas Chromatography/Mass Spectrometry (GC-MS)

Chromatograms were obtained from pore-filling oil residue to measure for m/z 85 (n-alkanes), 191 (hopanes) and 217 (steranes). The m/z 85 chromatogram (Figure 6) shows n-alkanes preserved to C26, but it is dominated by a large unresolved complex mixture (UCM). Individual hopanes and steranes were very clearly resolved and identified. The 20S/(20S + 20R) ratio, using $\alpha\alpha\alpha$ S and $\alpha\alpha\alpha$ R, for the C29 steranes is 0.69. The 22S/(22S + 22R) ratio for the C31 hopanes is 0.55.

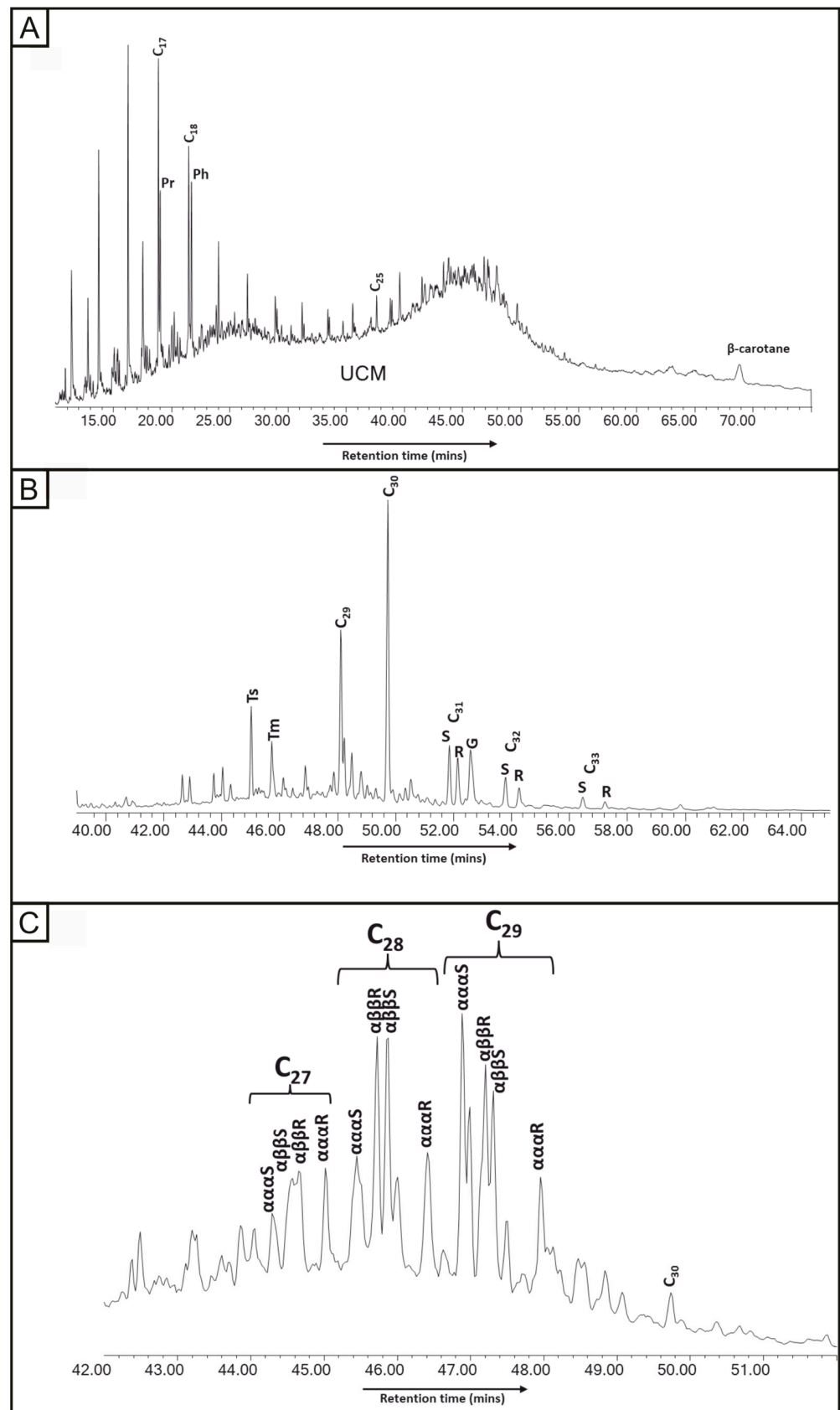


Figure 6. Mass chromatograms for oil residue in Yesnaby Sandstone. (A) m/z 85 n-alkane distribution with β -carotane (highlighted); (B) m/z 191 hopane distribution with gammacerane (highlighted); (C) m/z 217 sterane distribution.

5. Discussion

5.1. APS Minerals

Florencite is directly associated with bitumen nodules, occurring at the periphery of nodules (Figure 2A,B), in the Harra Ebb and Yesnaby sandstones. Goyazite predominantly occurs in illite matrices or as accessory minerals with bitumen, filling porosity (Figures 2C and 4A). The APS minerals lack heavy rare earth elements (HREE).

Illite cements appear to have mineralised in two phases, as part of a stable framework phase (Figure 7) that fills porosity in association with quartz overgrowths (Figure 2D), and a later mineralisation phase of illite infilling bitumen rim porosity coeval with pyrite (Figure 2B), florencite (Figure 2B) and goyazite (Figure 2C). Illite-associated florencite and goyazite minerals are also observed to crosscut uraniferous (Figure 2B) and non-uraniferous bitumen, supporting a distinct phase of illite mineralisation following the uranium mineralisation of pore-filling oil (Figure 7).

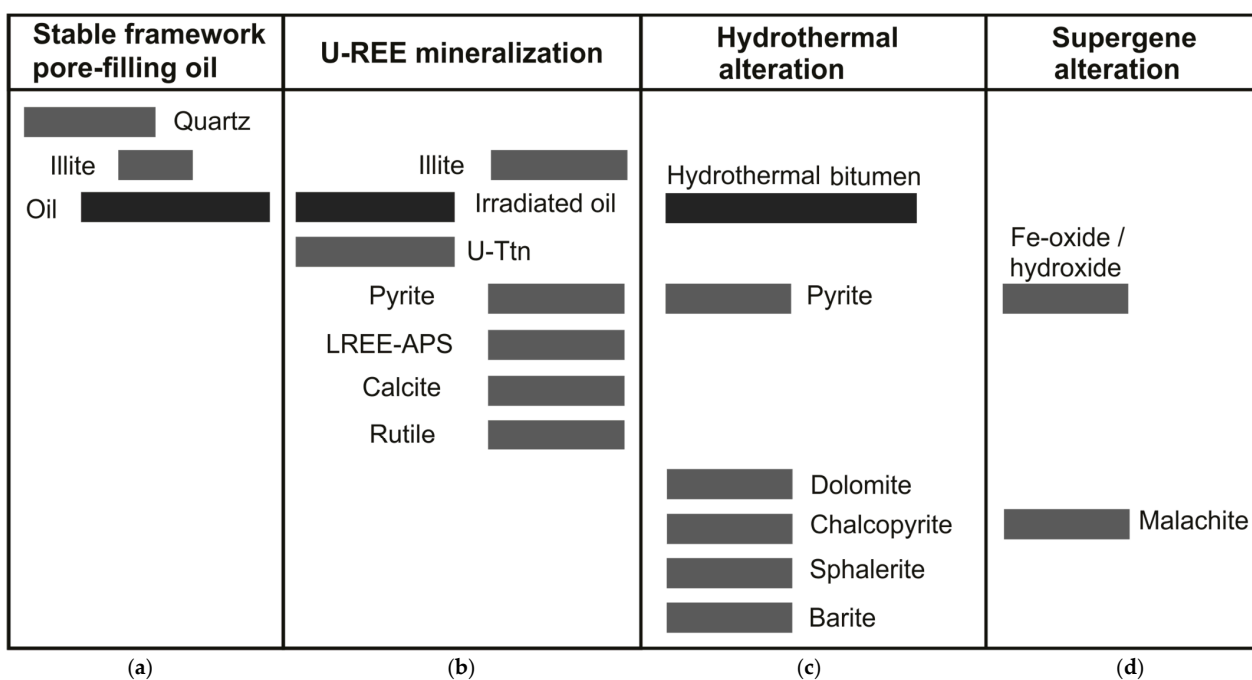


Figure 7. Paragenetic sequence for mineralised sandstone, Devonian, Yesnaby. The paragenetic phases are separated into (a) Diagenesis of authigenic minerals and oil charging of thermally mature hydrocarbons; (b) Brannerite (U-Ttn), rutile (Rt) and REE mineralisation accompanied by sulphide-mineralising fluids, calcite cementation and secondary illite formation; (c) Hydrothermal alteration by late-stage bitumen associated with Cu-Ba-Zn sulphides and dolomite mineralisation. (d) Supergene alteration during uplift and surface weathering, altering Cu-sulphides to malachite and pyrite to Fe oxide/hydroxide.

LREE-bearing APS grains associated with uraniferous hydrocarbons are similarly documented by [44] in the Franceville Basin, Gabon, in which they are inferred to have been deposited by the mixing of hydrocarbons with P, U and REE-bearing basinal fluids, following the dissolution of monazite by oxidised fluids. Bitumen was the main reductant in this model [8,44]. The reducing conditions of the Yesnaby oil reservoir, where florencite occurs, are comparable with the reduced, low pH and low oxygen fugacity conditions inferred for LREE-rich APS mineralisation by [17,18]. Florencite also occurs with uraniferous bitumen nodules in the Witwatersrand Supergroup [45], for which the Orkney nodules are considered to be an analogue [6]. More generally, the chemistry for APS formation was readily available. The lacustrine sediments that were the source of oil were also rich in both phosphorus and sulphur. The organic-rich horizons contain widespread phosphatic

remains of fish (bones, scales, coprolites) and the shallow water sediments contain extensive evidence of sulphate evaporites [46].

The S-Sr-LREE ternary plot (Figure 8) describes the compositional variability of APS minerals on the goyazite-florencite-svanbergite solid-solution series [18]. The compositions attributed to florencite and goyazite in this study are compared with APS mineral compositions from studies in different deposit types. LREE-rich APS minerals described by [18,22,26] are associated with oxidising, low pH physiochemical conditions that promote LREE solubility in F- or Cl- fluids, typically depositing LREE-APS minerals during late-stage hydrothermal alteration [17], or in proximity to altered U-unconformity mineralisation [18]. The florencite compositions measured in this study are most similar to moderately LREE-rich APS compositions of goyazite-florencite-svanbergite solid series reported in Baltic paleosol sediments [47] and in the Athabasca basin, moderately LREE-rich goyazite-svanbergite of distal and intermediate U-unconformity alteration zones [18] and moderately LREE-rich florencite in early-stage hydrothermal alteration assemblages [17].

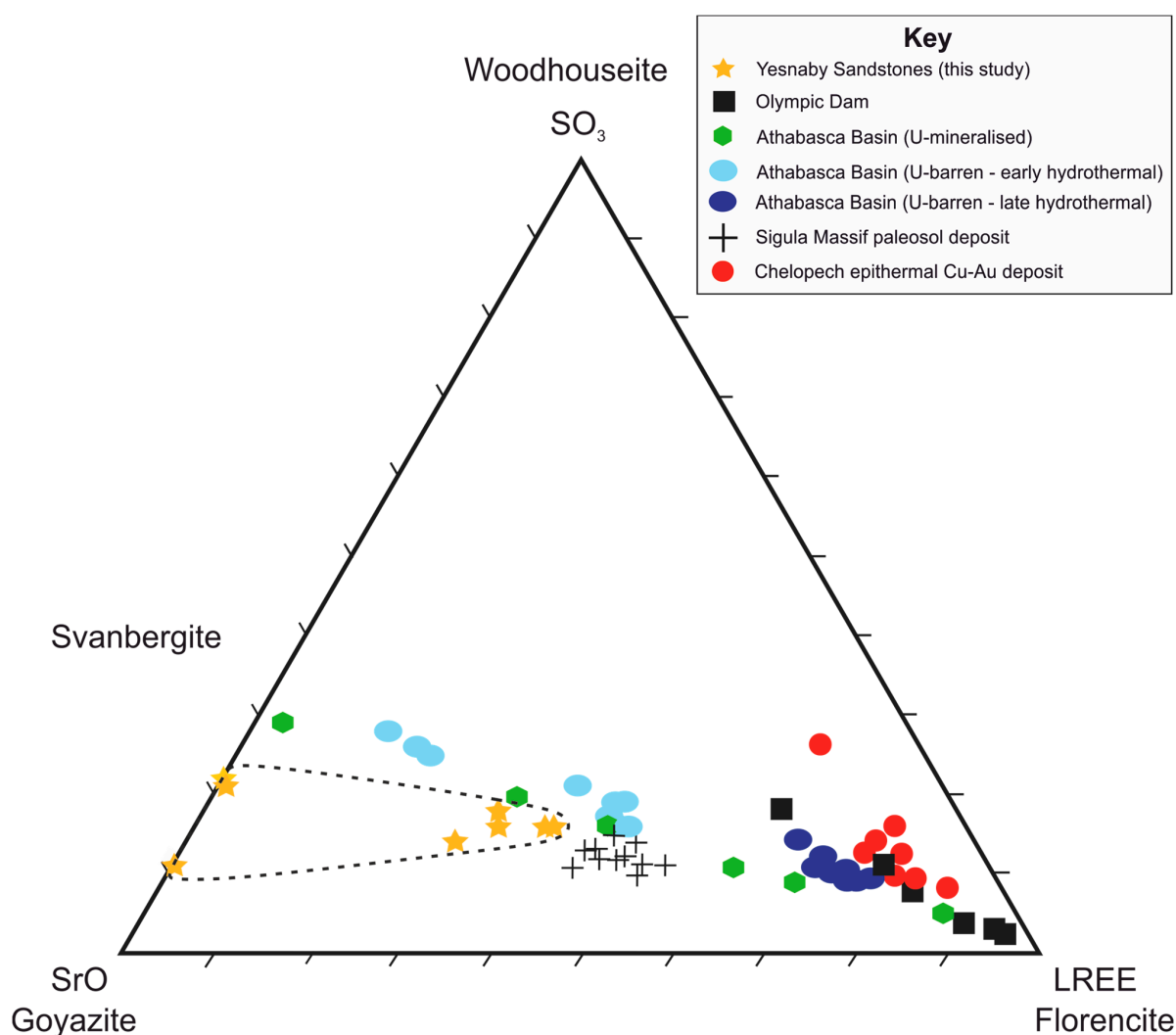


Figure 8. Ternary plot of LREE (Ce_2O_3 , La_2O_3 , Pr_2O_3 and Nd_2O_3), SO_3 and SrO, describing the compositional variability in florencite and goyazite from Yesnaby compared with literature data of LREE-APS compositions from different deposits. Yesnaby locality sandstone data (this study) are found within the dashed line, represented by yellow stars. Literature sources: Olympic Dam Cu-U-Au-Ag ore deposit [26], U-mineralised unconformity deposits [18] and U-barren, early and late hydrothermal alteration deposits [17] in the Athabasca Basin; Chelopech high-sulphidation epithermal Cu-Au deposit [22] and weathered Proterozoic crust (Baltic Paleosol) in the Sigula Massif [47].

5.2. Copper-Barite-Sphalerite Minerals

The isotope geochemistry, petrology and paragenesis of the Yesnaby sandstone are comparable to many other sedimentary-hosted copper oil deposits globally (Table 5). The combination of Cu-U-REE mineralisation is not uncommon; however, it is most often a feature of high-temperature deposition [48]. In other comparable deposits, early diagenetic haematite precipitation is followed by low-temperature hydrocarbon migration as burial depth increases. These reducing fluids commonly result in the ‘bleaching’ of the haematite, where the interaction between reduced iron from the haematite, and bacterially reduced sulphur, together form pyrite. A proportion of the soluble iron is also carried away in the reducing fluids. The presence of highly negative $\delta^{34}\text{S}$ values in all these deposits provides evidence of bacterial sulphate reduction (BSR) (Table 5). This is not, however, clear at Yesnaby, where the closed system of the lacustrine basin limited the isotopic fractionation that could occur, and allowed heavy residual sulphate to reprecipitate relatively heavy pyrite [49,50]. The aeolian depositional environment of the Yesnaby Sandstone Fm indicates that haematite grain coatings would have been present at the deposition. The lack of haematite coatings to detrital grains in these deposits today supports a model of diagenetic ‘bleaching’ (dissolution of haematite coating) during hydrocarbon migration.

Table 5. Comparison of sandstone-hosted copper-oil deposits globally, including Yesnaby, Orkney (this study). HC = Hydrocarbon, Hm = haematite, Py = Pyrite, Ccp = Chalcopyrite, Cal = Calcite, Bar = Barite. Simplified mineralisation paragenesis given for each deposit. Other global deposit data and parageneses collated from works as cited in locality column.

Locality	Host Rock Age	Cu (%)	Mineralisation Max T (°C)	Hydrocarbon Emplacement T (°C)	S-Isotopes ($\delta^{34}\text{S}$)	Mineralisation Paragenesis
Yesnaby, Orkney (This study)	Devonian Sandstone	>1%	190 °C	120–140 °C	+10.6‰ (py)	Hm → HC + Bar + Py → Cu + Zn
Paradox Basin, Colorado [12,51,52]	Permian to Cretaceous Sandstones	~4%	>120 °C	105–110 °C	−26.4 to +2.6‰ (py & ccp)	Hm → HC + Py → Cu ± U
Neuquen Basin, Argentina [11,53,54]	Jurassic to Cretaceous Sandstones	0.3–1.86%	170 °C	100–185 °C	−60.2 to +18.2‰ (Cu & Fe-sulphides)	Hm → HC + Py + Cal → Cu (V-U) + Pb + Zn + Cal
Manto-type deposits, Chile [8,9,55]	Jurassic to Cretaceous Volcanics & Sandstones	~1.5%	180 °C	134 °C	−50.4 to −0.6‰ (sulphides)	HC + Py + Cal → Cu (+Ag)
Chu-Sarysu Basin, Kazakhstan [10]	Upper Carboniferous Sandstones	0.85–1.7%	93 °C	150 °C	−20.1 to −4.7‰ (sulphides)	Hm → HC ± Py → Cu + Pb + Zn
White Pine Region, Michigan [7,56,57]	Mid-Proterozoic Sandstones and Shales	2.33–4.93%	70–100 °C	115–190 °C	−15.8 to +31.2‰ (sulphides)	HC → Cu + Cal (Py → Cu)

In other deposits, the introduction of higher-temperature Cu-bearing saline fluid commonly results in the replacement of the pyrite by copper-bearing sulphides, including chalcopyrite, chalcocite, covellite, and bornite. A similar replacement mechanism of pyrite by chalcopyrite and sphalerite has occurred in the hydrothermal barite + sulphide veins in the Yesnaby Sandstone Fm (Figure 3D). There are several examples at the White Pine mine, some Chilean Manto-type deposits, and in the Neuquen Basin of hydrocarbons

which acted as the primary reductant to facilitate Cu-mineralisation from the hydrothermal brines [7,9,11,53,54], which is also likely to have occurred at Yesnaby.

A final stage of supergene alteration of vein assemblage minerals during uplift and surface weathering by low-temperature oxidising fluids led to the formation of malachite (from chalcopyrite), and Fe-oxide/hydroxide (from pyrite) (Figure 7).

5.3. The Role of Oil Residues in Mineralisation

The paragenesis indicates that there were two stages when oil residues were associated with mineralisation. Uranium mineralised the rock after the initial oil charge. As the APS minerals are directly associated with the uranium-bitumen mixtures, they can be regarded as part of the first mineralising stage. The copper mineralisation was associated with a later stage when bitumen veins cut through the sandstone. The minor sphalerite was part of the copper mineralising stage. The two stages were distinct, and they reflect different processes.

The concentration of uranium by oil residues is a widespread phenomenon [58–60], based on the polymerisation of fluid hydrocarbons (oil, gas) that encounter irradiation from uranium and/or thorium. As at Yesnaby, this occurs particularly in continental sediments, where high Eh conditions allow the mobility of uranium. The solid products of the polymerisation exhibit several distinctive features, including polymer swelling due to the progressive addition of more hydrocarbons, the precipitation of uranium minerals (brannerite, uraninite, coffinite) within the bitumen, and radioactive blasting haloes in the surrounding grains due to irradiation over subsequent geological time [61]. Several other examples of uraniferous bitumen occur elsewhere in the Devonian sediments of northern Scotland [62–64].

The mechanism of formation means that the uraniferous bitumens are typically formed at oil window temperatures (~80 to 150 °C). Where the oil residues are abundant in continental sandstone reservoirs, the mobile uranium can lead to deposits on an economic scale [65,66].

The copper mineralisation occurred subsequently, unrelated to irradiation. As discussed, similar sandstone-hosted copper mineralisation occurs in association with oil residues in several other continental basins (Table 5). It is, therefore, valuable to identify whether specific aspects of the oil residues particularly enhanced mineralisation and how these compare to those at Yesnaby. Relevant characteristics include the reducing nature of the oil residues [53], a role for organic fluids in the transport of metals [67], and changes in permeability concomitant with biodegradation during uplift [68]. These factors contribute to a range of relationships between copper mineralisation and sedimentary organic matter (Table 6). The Devonian case study reported here describes mineralisation which was controlled by the reducing environment of the oil residue.

Table 6. Relationships between copper mineralisation and sedimentary organic matter.

Relationship between Oil Residue and Mineralisation	Relative Timing of Mineralisation of Ore and Oil	Environment of Mineralisation	Reference
Reducing template on oil residue	Post-oil	Any	[53]
Evaporite sequences source oil and sulphides	Any	Any	[69]
Rift basin mixed volcanic copper and lacustrine oil	Any	Terrestrial	[57]
Oil charge strips metallic grain coatings	Post-oil	Terrestrial	[70]
Metal transport in low-pH organic fluids	Any	Any	[67]
Permeability enhanced in uplifted reservoir	Post-oil	Any	[68]
Assimilation organics in magmas to precipitate sulphides	Any	Any	[71]

Both uranium and copper are mobile in oxidising conditions, so are available for interaction with oil residues in continental sandstones. However, at Yesnaby the interactions

occurred at different stages, at least in part due to the nature of the interaction (irradiation, reduction), but possibly also due to the timing of metal availability. The uranium is most likely to have been derived from the underlying granitic basement, while the copper could have been remobilised from Devonian lacustrine sediments [38].

5.4. Relationship between Basement and Mineralisation

A close spatial relationship between mineralisation and the surface of the underlying granitic basement may seem surprising, given that there was a time gap of over 50 million years between the granite age of about 430 Ma [32] and the generation of oil at about 360 Ma [33]. However, a comparable timing scenario is also found 100 km to the south where Lower Devonian sandstones occur unconformably on the c.420 Ma Helmsdale Granite, at Ousdale [62]. At Ousdale, the sandstones are similarly oil-bearing and similarly mineralised by copper-REE-uranium [62]. The combined evidence from Yesnaby and Ousdale suggests a mineralising legacy from the Late Caledonian granites, which is most likely to represent a thermal reactivation of the granites, perhaps triggered by coupled magmatism and shearing which continued further south in the Caledonides until at least 380 Ma [72]. Both granites are still outcrops of high heat production today [73].

5.5. Paragenetic Sequence and Temperature History

The petrographic observations can be summarised by a paragenetic sequence (Figure 7). Hydrocarbon-bearing mineralisation assemblages occur in two distinct stages with REE-uraniferous-bearing fluids preceding hydrothermal sulphides. Pore space contains a solid oil residue from initial oil charging. Quartz overgrowths that surround the pore space contain primary oil fluid inclusions, so oil was emplaced coeval with quartz cementation. The sandstone contains uraniferous bitumen nodules and hosts rutile and pyrite minerals at the nodule rim (Figures 2B and 4A). The relative timing of uranium mineralisation, hydrocarbon migration and bitumen nodule formation at Yesnaby is not completely clear, and [6] considered a complex paragenesis in which detrital titanium-bearing minerals were progressively altered by interaction with uranium, then hydrocarbons. There is, however, evidence which makes this sequence ambiguous:

- (i) Primary quartz overgrowths contain oil fluid inclusions, indicating oil was present during their formation.
- (ii) The bitumen nodules consistently contain arrays of brannerite inclusions that typically cause the polymerisation of hydrocarbons by ionising radiation [6,74].
- (iii) The brannerite arrays have only been observed within the bitumen nodules.

Allowing uncertainty about the origin of the titanium, the key point is that the bitumen nodules and the brannerite mineral phase appear to be interdependent, and they both post-dated oil emplacement in the reservoir.

The Middle Devonian lacustrine sediments were high-quality, oil-prone source rocks [35,75], so are the assumed source of the oil in the exhumed reservoir. The occurrences of gammacerane and β -carotane (Figure 6) in the oil residue are consistent with derivation from a lacustrine source, and these compounds occur also in the Middle Devonian sediments. The hopane and sterane thermal maturity parameters for the oil are at their maximum values, indicating that they had reached at least the upper part of the oil-generating window. The m/z 85 chromatogram shows a large unresolved complex mixture (Figure 6), in the exhumed reservoir. The transformation from oil to bitumen is due to biodegradation and not attributable to radiation. The hydrocarbon and aqueous inclusions give near-identical homogenisation temperatures of about 120 to 140 °C (Table 3). Their co-occurrence implies that no pressure correction is required [76]. The yellow fluorescence of the hydrocarbon inclusions indicates a liquid oil that was less viscous than the black vein bitumen that occurs later in the paragenesis. The evidence of low oil viscosity in bitumen veins suggests that biodegradation to solid bitumen occurred subsequently. This is a likely consequence of the uplift of the rocks to shallower depths, where they would encounter meteoric (aqueous) fluids.

The temperature history is constrained by the generation of oil, precipitation of quartz overgrowths in sandstone, the formation of barite-chalcopyrite-hydrocarbon veins, and the thermal maturity of the hydrocarbons (Figure 7). Measurements of temperature have been assessed from the likely temperature of reservoir oil, fluid inclusions in quartz overgrowths, and Raman spectroscopy of the bitumen. There are no differences in maximum temperature between the bitumen in the veins and the pore-fill bitumen in the host rocks. The temperature of the Yesnaby reservoir rock is most likely at or below 100 °C [77]. The three temperatures are ~100 °C, 120–140 °C (fluid inclusion analysis of quartz overgrowths), and ~190 °C (Raman analyses of bitumen) (Table 5). The three measurements represent progressive paragenetic stages (Figure 9), as oil was already present when the quartz overgrowths formed, sandstone rafts with quartz overgrowths were incorporated in the barite, and the pore-fill and vein bitumen recorded the maximum thermal maturity.

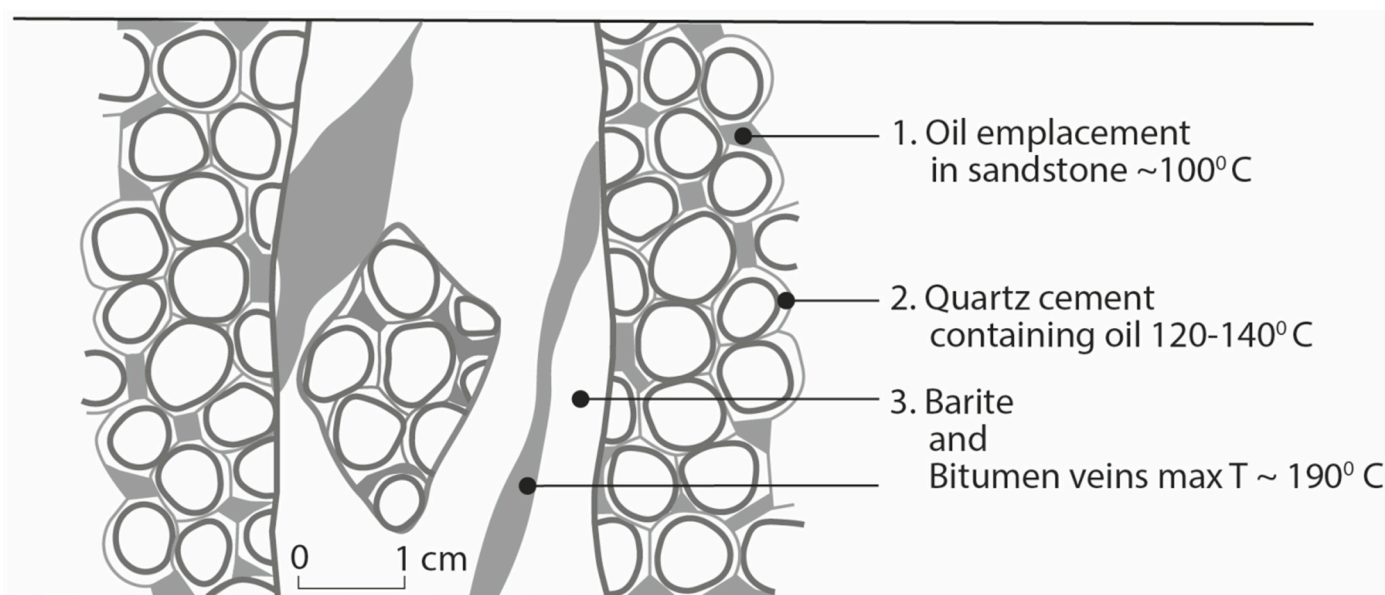


Figure 9. Schematic images of oil temperature history in sandstone, quartz cement and barite-bitumen hydrothermal veins.

All of the stages of diagenesis and mineralisation occurred at depth, as evidenced by the fluid inclusion and Raman spectroscopy data which suggest burial of at least 3 km. This depth is calculated using a geothermal gradient of 40 °C/km during the Devonian and then 20 °C/km thereafter [33]. Mineralisation was, therefore, complete before the uplift event during the end-Carboniferous to early Permian Hercynian Orogeny. Burial history reconstructions [3,33,78] show that oil had been generated during the latest Devonian-early Carboniferous, so are consistent with the later exhumation and biodegradation of oil reservoirs in the Orcadian Basin during the uplift event [79,80].

6. Conclusions

The mineralisation in a Devonian sandstone-hosted oil reservoir at Yesnaby, Orkney (Yesnaby Sandstone Fm and Harra Ebb Fm), includes copper-barite veining, REE-bearing APS minerals, and uranium as brannerite. A petrographic study of the deposit shows several aspects of the relationship between the mineralisation and oil residues:

- (i) All mineralisation is spatially associated with bitumen in the sandstone.
- (ii) All mineralisation postdated oil charging of the reservoir, i.e., oil emplacement occurred first.
- (iii) The mineralisation all occurred in the temperature range of 100 to ~190 °C

- (iv) Mineralisation occurred prior to biodegradation, which may have occurred during uplift. The role of exhumation, in this case is, therefore, the disposition of the deposit at the present surface rather than a genetic role in mineralisation.

The evidence documented here suggests that the formation of APS-copper mineralisation at Yesnaby occurred at temperatures relatively low compared with most previously documented occurrences.

As similar sandstone-hosted copper mineralisation occurs in association with oil residues in several other continental basins, it is valuable to identify whether specific aspects of the oil residues promoted mineralisation. Possible characteristics include the reducing nature of the oil residues, the role of organic fluids in the transport of metals, and changes in permeability concomitant with biodegradation during uplift. In the Yesnaby case, the timing of mineralisation between the emplacement of bitumen and uplift suggests that the reducing environment conferred by the oil was the predominant factor that favoured ore mineral deposition.

This conclusion implies that the distribution of oil reservoirs at shallow depths is a factor that should be incorporated into the exploration of copper deposits. Given that oil deposits occur in a range of structural and stratigraphic traps, the prediction of such traps would contribute to the exploration strategy. The traditional seismic-based methodologies used in oil exploration would thereby have a role in the search for copper resources.

Author Contributions: Conceptualisation, J.P. and E.A.H.; methodology, J.P., E.A.H. and J.G.T.A.; validation, J.P., J.G.T.A. and E.A.H.; formal analysis, E.A.H., J.G.T.A., J.P., A.S. and T.O.A.; investigation, E.A.H., J.P. and J.G.T.A.; resources, J.P.; data curation, E.A.H., J.G.T.A., J.P., A.S. and T.O.A.; writing—original draft preparation, E.A.H., J.P. and J.G.T.A.; writing—review and editing, J.P., J.G.T.A., E.A.H., A.S. and T.O.A.; visualisation, E.A.H. and J.P.; supervision, J.P.; project administration, J.P. and E.A.H.; funding acquisition, J.P. and E.A.H. All authors have read and agreed to the published version of the manuscript.

Funding: J.G.T.A. is supported by the Natural Environment Research Council (grant NE/T003677/1).

Data Availability Statement: All data and results presented within this article are provided in the text and associated figures/tables.

Acknowledgments: Skilled technical support was provided by J. Bowie, C. Taylor and J. Still.

Conflicts of Interest: The authors declare no conflict of interest. The funders had no role in the design of the study; in the collection, analyses, or interpretation of data; in the writing of the manuscript; or in the decision to publish the results.

References

1. Michie, U.M.L.; Cooper, D.C. Uranium in the Old Red Sandstone of Orkney. *Rep. Inst. Geol. Sci.* **1979**, *78*, 16.
2. Trewin, N.H. The petroleum potential of the Old Red Sandstone of northern Scotland. *Scott. J. Geol.* **1989**, *25*, 201–225. [[CrossRef](#)]
3. Brown, J.F.; Astin, T.R.; Marshall, J.E.A. The Paleozoic petroleum system in the north of Scotland—outcrop analogues. *Geol. Soc. Lond. Spec. Publ.* **2018**, *471*, 253–280. [[CrossRef](#)]
4. Mykura, W. Orkney and Shetland. In *British Regional Geology*; Her Majesty's Stationery Office: Edinburgh, UK, 1976.
5. Watson, J.V.; Plant, J. Regional geochemistry of uranium as a guide to deposit formation. *Philos. Trans. R. Soc. Lond. Ser. A* **1979**, *291*, 321–338.
6. McCready, A.J.; Parnell, J. A Phanerozoic analogue for Witwatersrand-type uranium mineralization: Uranium-titanium-bitumen nodules in Devonian conglomerates/sandstones, Orkney, Scotland. *Trans IMM (Sect. B Appl. Earth Sci.)* **1998**, *107*, 889–897.
7. Mauk, J.L.; Hieshima, G.B. Organic matter and copper mineralization at White Pine, Michigan, U.S.A. *Chem. Geol.* **1992**, *99*, 189–211. [[CrossRef](#)]
8. Cisternas, M.E.; Hermosilla, J. The role of bitumen in strata-bound copper deposit formation in the Copiapo area, Northern Chile. *Miner. Depos.* **2006**, *41*, 339–355. [[CrossRef](#)]
9. Wilson, N.S.F.; Zentilli, M. Association of pyrobitumen with copper mineralization from the Uchumi and Talcuna districts, central Chile. *Int. J. Coal Geol.* **2006**, *65*, 158–169. [[CrossRef](#)]
10. Box, S.E.; Syusyura, B.; Hayes, T.S.; Taylor, C.D.; Zientek, M.L.; Hitzman, M.W.; Seltmann, R.; Chechetkin, V.; Dolgopolova, A.; Cossette, P.M.; et al. Sandstone Copper Assessment of the Chu-Sarysu Basin, Central Kazakhstan. In *U.S. Department of the Interior, U.S. Geological Survey, Scientific Investigations Report 2010-5090-E*; U.S. Department of the Interior: Washington, DC, USA, 2012.

11. Pons, M.J.; Franchini, M.; Giusiano, A.; Patrier, P.; Beaufort, D.; Impiccini, A.; Rainoldi, A.L.; Meinert, L. Alteration halos in the Tordillos sediment-hosted copper deposit of the Neuquen Basin, Argentina. *Ore Geol. Rev.* **2017**, *80*, 691–715. [[CrossRef](#)]
12. Barton, I.F.; Barton, M.D.; Thorson, J.P. Characteristics of Cu and U-V Deposits in the Paradox Basin (Colorado Plateau) and associated alteration. *Soc. Econ. Geol. Inc. Guideb. Ser.* **2018**, *59*, 73–102.
13. Dill, H.G. The geology of aluminium phosphates and sulphates of the alunite group minerals: A review. *Earth-Sci. Rev.* **2001**, *53*, 35–93. [[CrossRef](#)]
14. Xu, X.-W.; Mao, Q.; Li, X.-H.; Pirajno, F.M.; Qu, X.; Deng, G.; Chen, D.-Z.; Zhang, B.-L.; Dong, L.-H. Copper-Zinc albite porphyry in the Hersai porphyry copper deposit, East Junggar, China: A transition between late magmatic and hydrothermal porphyry copper deposit. *Ore Geol. Rev.* **2014**, *61*, 141–156. [[CrossRef](#)]
15. Kovács, I.; Németh, T.; Kiss, G.B.; Kis, V.K.; Tóth, Á.; Benkó, Z. Rare aluminium phosphates and sulphates (APS) and clay mineral assemblages in silicified hydraulic breccia hosted by a Permian granite (Velence Mts., Hungary) as indicators of a high sulfidation type epithermal system. *Mineral. Petrol.* **2019**, *113*, 217–228. [[CrossRef](#)]
16. Martínez, J.C.; Dristas, J.A.; Massonne, H.J.; Theye, T. Alunite and REE rich APS minerals associated to the hydrothermal clay deposits in the Barker area, Tandilia, Argentina. *Clay Sci.* **2006**, *12* (Suppl. 2), 15–20.
17. Cloutier, J.; Kyser, K.; Olivo, G.R.; Alexandre, P. Contrasting patterns of alteration at the Wheeler River area, Athabasca Basin, Saskatchewan, Canada: Insights into the apparently Uranium-barren zone K alteration system. *Econ. Geol.* **2010**, *105*, 303–324. [[CrossRef](#)]
18. Gaboreau, S.; Cuney, M.; Quirt, D.; Beaufort, D.; Patrier, P.; Matthew, R. Significance of aluminium phosphate-sulfate minerals associated with Unconformity-type deposits: The Athabasca Basin, Canada. *Am. Mineral.* **2007**, *92*, 267–280. [[CrossRef](#)]
19. Riegler, T.; Quirt, D.; Beaufort, D. Spatial distribution and compositional variation of APS minerals related to uranium deposits in the Kiggavik-Andrew Lake structural trend, Nunavut, Canada. *Miner. Depos.* **2016**, *51*, 219–236. [[CrossRef](#)]
20. Rojkovič, I.; Konečný, P.; Novotný, L.; Puškelová, L.; Streško, V. Quartz-Apatite-REE vein mineralization in early paleozoic rocks of the Gemeric Superunit, Slovenia. *Geol. Carpathica* **1999**, *50*, 215–227.
21. Hikov, A. First find of florencite-(Ce,La,Nd) in advanced argillic altered rocks from the Asarel porphyry copper deposit, Central Srednogori. *Rev. Bulg. Geol. Soc.* **2017**, *80*, 33–35.
22. Georgieva, S.; Velinova, N. Florencite-(Ce, La, Nd) and crandallite from the advanced argillic alteration in the Chelopech high-sulphidation epithermal Cu-Au deposit, Bulgaria. *Comptes Rendus L'académie Bulg. Des Sci.* **2014**, *67*, 1669–1678.
23. Lefebvre, J.J.; Patterson, L.E. Hydrothermal assemblages of aluminian serpentine, florencite and kyanite in the Zairian Copperbelt. *Ann. Société Géologique Belg.* **1982**, *105*, 51–71.
24. Chakraborty, M.; Biswas, S.; Sengupta, N.; Sengupta, P. First report of florencite from the Singhbhum Shear Zone of the East Indian Craton. *Int. J. Mineral.* **2014**, *2014*, 978793. [[CrossRef](#)]
25. Davidson, G.J.; Paterson, H.; Meffre, S.; Berry, R.F. Characteristics and origin of the Oak Dam East breccia-hosted, iron oxide Cu-U-(Au) Deposit: Olympic Dam Region, Gawler Craton, South Australia. *Econ. Geol.* **2007**, *102*, 1471–1498. [[CrossRef](#)]
26. Schmandt, D.S.; Cook, N.J.; Ciobanu, C.L.; Ehrig, K.; Wade, P.W.; Gilbert, S.; Kamenetsky, V.S. Rare earth element phosphate minerals from the Olympic Dam Cu-U-Au-Ag deposit, South Australia: Recognizing temporal-spatial controls on REE mineralogy in an evolved IOCG system. *Can. Mineral.* **2019**, *57*, 1–22. [[CrossRef](#)]
27. Khashgerel, B.-E.; Kavalieris, I.; Hayashi, K.-I. Mineralogy, textures, and whole-rock geochemistry of advanced argillic alteration: Hugo Dummett porphyry Cu-Au deposit, Oyu Tolgoi mineral district, Mongolia. *Miner. Depos.* **2008**, *43*, 913–932. [[CrossRef](#)]
28. Stoffregen, R.E.; Alpers, C.N. Woodhouseite and svanbergite in hydrothermal ore deposits: Products of apatite destruction during advanced argillic alteration. *Can. Mineral.* **1987**, *25*, 201–211.
29. Soroka, E.I.; Leonova, L.V.; Pritchyn, M.E. Brockite in wallrock metasomatites of the Safyanovskoe copper-sulphide deposit (Middle Urals). *News Ural. State Min. Univ.* **2020**, *3*, 35–40. [[CrossRef](#)]
30. Voudouris, P.C.; Melfos, V. Aluminum-phosphate-sulfate (APS) minerals in the sericitic-advanced argillic alteration zone of the Melitena porphyry-epithermal Mo-Cu ± Au ± Re prospect, western Thrace, Greece. *Neues Jahrb. Mineral. Abh.* **2012**, *190*, 11–27. [[CrossRef](#)] [[PubMed](#)]
31. Strachan, R.A. The metamorphic basement geology of Mainland Orkney and Graemsay. *Scott. J. Geol.* **2003**, *39*, 145–149. [[CrossRef](#)]
32. Lundmark, A.M.; Augland, L.E.; Bjerga, A.D. Timing of strain partitioning and magmatism in the Scottish Scandian collision, evidence from the high Ba-Sr Orkney granite complex. *Scott. J. Geol.* **2019**, *55*, 21–34. [[CrossRef](#)]
33. Parnell, J.; Carey, P.; Monson, B. Timing and temperature of décollement on hydrocarbon source rock beds in cyclic lacustrine successions. *Palaeogeogr. Palaeoclimatol. Palaeoecol.* **1998**, *140*, 121–134. [[CrossRef](#)]
34. Dichiarante, A.M.; Holdsworth, R.E.; Dempsey, E.D.; Selby, D.; McCaffrey, K.J.W.; Michie, U.M.L.; Morgan, G.; Boniface, J. New structural and Re-Os geochronological evidence constraining the age of faulting and associated mineralization in the Devonian Orcadian basin, Scotland. *J. Geol. Soc.* **2016**, *173*, 457–473. [[CrossRef](#)]
35. Ghazwani, A.; Littke, R.; Sachse, V.; Fink, R.; Mahlstedt, N.; Hartkopf-Fröder, C. Organic geochemistry, petrology and palynofacies of Middle Devonian lacustrine flagstones in the Orcadian Basin, Scotland: Depositional environment, thermal history and petroleum generation potential. *Geol. Mag.* **2018**, *155*, 773–796. [[CrossRef](#)]
36. Gallagher, M.J.; Michie, U.M.; Smith, R.T.; Haynes, L. New evidence of uranium and other mineralization in Scotland. *Trans. Inst. Min. Metall.* **1971**, *80*, 150–173.

37. Plant, J.A.; Forrest, M.D.; Hodgson, J.F.; Smith, R.T.; Stevenson, A.G. Regional geochemistry in the detection and modelling of mineral deposits. In *Applied Geochemistry in the 1980s*; Thornton, I., Howarth, R.J., Eds.; Graham and Trotman: London, UK, 1986; pp. 103–139.
38. Muir, R.O.; Ridgway, J.M. Sulphide mineralisation of the continental Devonian sediments of Orkney (Scotland). *Miner. Depos.* **1975**, *10*, 205–215. [[CrossRef](#)]
39. Parnell, J. Mineralized Magadi-type cherts in the Devonian of Scotland: Support for a model of sulfide deposition in low-temperature alkaline conditions. *Econ. Geol.* **1987**, *82*, 1053–1056. [[CrossRef](#)]
40. Parnell, J.; Janaway, T. Sulphide-mineralized algal breccias in a Devonian evaporitic lake system, Orkney, Scotland. *Ore Geol. Rev.* **1990**, *4*, 445–460. [[CrossRef](#)]
41. Peters, K.E.; Walters, C.C.; Moldowan, J.M. The Biomarker Guide. In *Biomarkers and Isotopes in Petroleum Exploration and Earth History*; Cambridge University Press: Cambridge, UK, 2005.
42. Lünsdorf, N.K.; Lünsdorf, J.O. Evaluating Raman spectra of carbonaceous matter by automated, iterative curve-fitting. *Int. J. Coal Geol.* **2016**, *160*, 51–62. [[CrossRef](#)]
43. Lünsdorf, N.K.; Dunkl, I.; Schmidt, B.C.; Rantitsch, G.; Von Eynatten, H. Towards a higher comparability of geothermometric data obtained by Raman spectroscopy of carbonaceous material. Part 2: A revised geothermometer. *Geostand. Geoanalytical Res.* **2017**, *41*, 593–612. [[CrossRef](#)]
44. Lecomte, A.; Michels, R.; Cathelineau, M.; Mortol, C.; Brousand, M.; Flotte, N. Uranium deposits of Franceville Basin (Gabon): Role of organic matter and oil cracking on uranium mineralization. *Ore Geol. Rev.* **2020**, *123*, 103579. [[CrossRef](#)]
45. Fuchs, S.; Schumann, D.; Martin, R.F.; Couillard, N. The extensive hydrocarbon-mediated fixation of hydrothermal gold in the Witwatersrand Basin, South Africa. *Ore Geol. Rev.* **2021**, *138*, 104313. [[CrossRef](#)]
46. Astin, T.R.; Rogers, D.A. Subaqueous shrinkage cracks in the Devonian of Scotland reinterpreted. *Scott. J. Geol.* **1991**, *61*, 850–859.
47. Vircava, I.; Somelar, P.; Liivamägi, S.; Kirs, J.; Kirsimäe, K. Origin and paleoenvironmental interpretation of aluminium phosphate sulfate minerals in a Neoproterozoic Baltic paleosol. *Sediment. Geol.* **2015**, *319*, 114–123. [[CrossRef](#)]
48. Baidya, A.S.; Pal, D.C. Geochemical evolution and timing of uranium mineralization in the Khetri Coppe Belt, western India. *Ore Geol. Rev.* **2020**, *127*, 193974. [[CrossRef](#)]
49. Jørgensen, B.B.; Böttcher, M.E.; Lüschen, H.; Neretin, L.N.; Volkov, I.I. Anaerobic methane oxidation and a deep H₂S sink generate isotopically heavy sulfides in Black Sea sediments. *Geochim. Et Cosmochim. Acta* **2004**, *68*, 2095–2118. [[CrossRef](#)]
50. Lin, Z.; Sun, X.; Peckmann, J.; Lu, Y.; Xu, L.; Strauss, H.; Zhou, H.; Gong, J.; Lu, H.; Teichert, B.M.A. How sulfate-driven anaerobic oxidation of methane affects the sulfur isotopic composition of pyrite: A SIMS study from the South China Sea. *Chem. Geol.* **2016**, *440*, 26–41. [[CrossRef](#)]
51. Kim, J.H.; Bailey, L.; Noyes, C.; Tyne, R.L.; Ballentine, C.J.; Ma, L.; Barton, M.; Barton, L.; Reiners, P.W.; Ferguson, G.; et al. Hydrogeochemical evolution of formation waters responsible for sandstone bleaching and ore mineralization in the Paradox Basin, Colorado Plateau, USA. *Bull. Geol. Soc. Am.* **2022**, *134*, 2589–2610. [[CrossRef](#)]
52. Macintyre, T.J.; Hitzman, M.W.; Thorson, J.P. Hydrocarbon-induced bleaching and copper mineralization in the Wingate Sandstone, Paradox Valley, Colorado: Two episodes of fluid migration during the evolution of the Paradox Basin. *AAPG Bull.* **2022**, *107*, 169–189. [[CrossRef](#)]
53. Rainoldi, A.L.; Franchini, M.B.; Boyce, A.J.; Giusiano, A.; Cesaretti, N.N.; Pons, J.; Ríos, F.J. Stable isotope and fluid inclusion study of sediment-hosted stratiform copper deposits from the Neuquén Basin, Argentina. *Miner. Depos.* **2019**, *54*, 415–436. [[CrossRef](#)]
54. Pons, M.J.; Franchini, M.; Rainoldi, A.L.; Giusiano, A.; Cesaretti, N.N.; Montagna, A.O.; Herrington, R. Base metal mobility linked to brine and hydrocarbon migration at the Huincul High in the Neuquén Basin, Argentina: Implications for the formation of sediment-hosted base metal deposits. *J. Geochem. Explor.* **2021**, *226*, 106778. [[CrossRef](#)]
55. Carrillo-Rosúa, J.; Boyce, A.J.; Morales-Ruano, S.; Morata, D.; Roberts, S.; Munizaga, F.; Moreno-Rodríguez, V. Extremely negative and inhomogeneous sulfur isotope signatures in Cretaceous Chilean manto-type Cu-(Ag) deposits, Coastal Range of central Chile. *Ore Geol. Rev.* **2014**, *56*, 13–24. [[CrossRef](#)]
56. Burnie, S.W.; Schwarcz, H.P.; Crocket, J.H. A Sulfur Isotopic Study of the White Pine Mine, Michigan. *Econ. Geol.* **1972**, *67*, 895–914. [[CrossRef](#)]
57. Ho, E.S.; Mauk, J.U. Relationship between organic matter and copper mineralization in the Proterozoic Nonesuch Formation, northern Michigan. *Ore Geol. Rev.* **1996**, *11*, 71–87. [[CrossRef](#)]
58. Leventhal, J.S.; Daws, T.A.; Frye, J.S. Organic geochemical analysis of sedimentary organic matter associated with uranium. *Appl. Geochem.* **1986**, *1*, 241–247. [[CrossRef](#)]
59. Kříbek, B.; Žák, K.; Spangenberg, J.E.; Jehlička, J.; Prokeš, S.; Komínek, J. Bitumens in the late Variscan hydrothermal vein-type uranium deposit of Příbram, Czech Republic: Sources, Radiation-Induced Alteration and Relation to Mineralization. *Econ. Geol.* **1999**, *94*, 1093–1114. [[CrossRef](#)]
60. Alexandre, P.; Kyser, T.K. Geochemistry of uraniumiferous bitumen in the southwest Athabasca Basin, Saskatchewan, Canada. *Econ. Geol.* **2006**, *101*, 1605–1612. [[CrossRef](#)]
61. Parnell, J.; Monson, B.; Tosswill, R.J. Petrography of thoriferous hydrocarbon nodules in sandstones, and their significance for petroleum exploration. *J. Geol. Soc. Lond.* **1990**, *147*, 837–842. [[CrossRef](#)]
62. Pointer, C.M.; Ashworth, J.R.; Simpson, P.R. Genesis of coffinite and the U-Ti association in Lower Old Red sandstone sediments, Ousdale, Caithness, Scotland. *Miner. Depos.* **1989**, *24*, 117–123. [[CrossRef](#)]

63. Tweedie, J.R. Origin of uranium and other metal enrichments in the Helmsdale Granite, eastern Sutherland, Scotland. *Trans. Inst. Min. Metallurgy. Sect. B Appl. Earth Sci.* **1979**, *88*, B145–B153.
64. Parnell, J.; Eakin, P. The replacement of sandstones by uraniumiferous hydrocarbons: Significance for petroleum migration. *Mineral. Mag.* **1987**, *51*, 505–515. [[CrossRef](#)]
65. Salas, J.; Bitzer, K.; Ayora, C. Origin and genesis of the Oklo uranium ore deposits (Gabon): Results from a basin scale fluid flow modelling. *J. Geochem. Explor.* **2000**, *69–70*, 165–171. [[CrossRef](#)]
66. Jaireth, S.; McKay, A.; Lambert, I. Association of large sandstone uranium deposits with hydrocarbons. *AUSGEO News* **2008**, *89*, 1–6.
67. Saintilan, N.J.; Spangenberg, J.E.; Chiaradia, M.; Chelle-Michou, C.; Stephens, M.B.; Fontboté, L. Petroleum as source and carrier of metals in epigenetic sediment-hosted mineralization. *Sci. Rep.* **2019**, *9*, 8283. [[CrossRef](#)]
68. Parnell, J. Diagenesis and fluid flow in response to uplift and exhumation. *Geol. Soc. Lond. Spec. Publ.* **2002**, *196*, 433–446. [[CrossRef](#)]
69. Warren, J.K. Evaporites, brines and base metals: Low-temperature ore emplacement controlled by evaporite diagenesis. *Aust. J. Earth Sci.* **2000**, *47*, 179–208. [[CrossRef](#)]
70. Parnell, J.; Wang, X.; Raab, A.; Feldmann, J.; Brolly, C.; Michie, R.; Armstrong, J. Metal flux from dissolution of iron oxide grain coatings in sandstones. *Geofluids* **2021**, *2021*, 5513490. [[CrossRef](#)]
71. Armstrong, J.G.T.; Parnell, J.; Boyce, A.J. Carbon in Mineralised Plutons. *Geosciences* **2022**, *12*, 202. [[CrossRef](#)]
72. Miles, A.J.; Woodcock, N.H.; Hawkesworth, C.J. Tectonic controls on post-subduction granite genesis and emplacement: The late Caledonian suite of Britain and Ireland. *Gondwana Res.* **2016**, *39*, 250–260. [[CrossRef](#)]
73. Gillespie, M.R.; Crane, E.J.; Barron, H.F. Deep Geothermal Energy Potential in Scotland. In *British Geological Survey Commissioned Report*; British Geological Survey: Keyworth, UK, 2013.
74. Ashfaq, A.; Clochard, M.C.; Coqueret, X.; Dispenza, C.; Driscoll, M.S.; Ulański, P.; Al-Sheikhly, M. Polymerization reactions and modifications of polymers by ionizing radiation. *Polymers* **2020**, *12*, 2877. [[CrossRef](#)]
75. Parnell, J.; Rahman, M. Source-rock evaluation of Devonian lacustrine carbonates, northern Scotland. *AAPG Bull.* **1990**, *74*, 345–351.
76. Goldstein, R.H.; Reynolds, T.J. Systematics of fluid inclusions in diagenetic minerals. In *SEPM Short Course No. 31*; SEPM: Tulsa, OK, USA, 1994; p. 199.
77. Bjørkum, P.A.; Nadeau, P.H. Temperature controlled porosity/permeability reduction, fluid migration, and petroleum exploration in sedimentary basins. *APPEA J.* **1998**, *38*, 453–464. [[CrossRef](#)]
78. Hillier, S.; Marshall, J.E.A. Organic maturation, thermal history and hydrocarbon generation in the Orcadian Basin, Scotland. *J. Geol. Soc.* **1992**, *149*, 491–502. [[CrossRef](#)]
79. Hippler, S.J. Deformation microstructures and diagenesis in sandstone adjacent to an extensional fault: Implications for the flow and entrapment of hydrocarbons. *AAPG Bull.* **1993**, *77*, 625–637.
80. Baba, M.; Parnell, J.; Muirhead, D.; Bowden, S. Oil charge and biodegradation history in an exhumed fractured reservoir, Devonian, UK. *Mar. Pet. Geol.* **2019**, *101*, 281–289. [[CrossRef](#)]

Disclaimer/Publisher’s Note: The statements, opinions and data contained in all publications are solely those of the individual author(s) and contributor(s) and not of MDPI and/or the editor(s). MDPI and/or the editor(s) disclaim responsibility for any injury to people or property resulting from any ideas, methods, instructions or products referred to in the content.